Eur J Vasc Endovasc Surg (2019) 57, 709–718

Haemodynamics in Different Flow Lumen Configurations of Customised Aortic Repair for Infrarenal Aortic Aneurysms

Simon P. Overeem [a,b,*], Jean-Paul P.M. de Vries [c], Jorrit T. Boersen [a], Cornelis H. Slump [d], Michel M.P.J. Reijnen [b,e], Michel Versluis [b,f], Erik Groot Jebbink [b]

[a] Department of Vascular Surgery, St. Antonius Hospital, Nieuwegein, the Netherlands
[b] Multimodality Medical Imaging M3i Group, Technical Medical Centre, University of Twente, the Netherlands
[c] Division of Surgery, Department of Vascular Surgery, University Medical Centre Groningen, Groningen, the Netherlands
[d] Robotics and Mechatronics, Technical Medical Centre, University of Twente, Enschede, the Netherlands
[e] Department of Vascular Surgery, Rijnstate Hospital, Arnhem, the Netherlands
[f] Physics of Fluids Group, University of Twente, Enschede, the Netherlands

WHAT THIS PAPER ADDS

This paper investigates the haemodynamics in three different flow lumen configurations of a custom, non-contained, non-cross linked polymer based endovascular approach in treating abdominal aortic aneurysms. The most favourable configuration was established by identifying flow velocity, vorticity, wall shear stress, and time averaged wall shear stress in an *in vitro* set up with laser particle imaging velocimetry. Based on the results, future research should focus on clinical applicability.

Objective: Customised aortic repair (CAR) is a new and minimally invasive technique for the endovascular treatment of abdominal aortic aneurysms (AAAs). The aneurysm is completely sealed with a non-contained, non-cross linked polymer, while a new flow lumen is created with balloons. For CAR, the haemodynamically most favourable balloon and flow lumen configuration has not been established before; therefore, four flow parameters were assessed in an *in vitro* model.

Methods: Three *in vitro* balloon configurations were implanted in an *in vitro* AAA model; a configuration with crossing balloons (CC) and two parallel configurations (PC1 and PC2). These three models were consecutively placed in a flow system that mimics physiological flow conditions. Laser particle imaging velocimetry (PIV) was used to resolve spatial and temporal flow patterns during the cardiac cycle. In house built algorithms were used to analyse the PIV data for the computing of (i) flow velocity; (ii) vorticity; (iii) wall shear stress (WSS); and (iv) time averaged wall shear stress (TAWSS).

Results: Suprarenal flow patterns were similar in all models. The CC showed a higher infrarenal velocity than PC1 and PC2 (38 cm/s vs. 23 cm/s vs. 23 cm/s), and a higher vorticity at the crossing of the lumens (CC: 337/s; PC1 127/s; PC2: 112/s). The lowest vorticity was observed in PC2, especially in the infrarenal neck (CC: 200/s; PC1 164/s; PC2: 98/s). Although WSS and TAWSS varied between configurations, values were in the within non-pathological range.

Conclusion: The flow lumens created by three balloon configurations used in an *in vitro* model of CAR have been studied, and resulted in different haemodynamics. The differences in velocity and lower vorticity, especially at the crossing section of the two balloons, showed that PC2 has favourable haemodynamics compared with the CC and PC1. Future research will be focused on the clinical applicability of CAR based on the PC2 design.

Keywords: AAA, Polymer, Haemodynamics, In vitro, Laser particle imaging velocimetry
Article history: Received 21 June 2018, Accepted 20 November 2018, Available online 15 April 2019

INTRODUCTION

Since the introduction of the endovascular aortic repair (EVAR) procedure in 1991 by Parodi *et al.*,[1] a large variety of endoprostheses have been introduced.[2,3] EVAR devices underwent evolution rather than revolution, while still improving clinical outcome.[4] Tadros *et al.* showed that re-intervention rates after EVAR declined from 33% in the first five years after implantation of EVAR, to 10% after 2008.[5] Despite this success rate, the 15 year re-intervention rate after EVAR, with the use of first generation devices, was 26%, according to the EVAR-1 investigators, vs. 12% in the open repair group.[6] Meta-analysis of the EVAR-1, DREAM, OVER, and ACE trials by Powell *et al.* showed

* Corresponding author. Multimodality Medical Imaging M3i group, Technical Medical Centre, University of Twente, Drienerlolaan 5, 7522 NB, Enschede, the Netherlands.
E-mail address: s.p.overeem@utwente.nl (Simon P. Overeem).
1078-5884/
https://doi.org/10.1016/j.ejvs.2018.11.012

that type II endoleak is the most common complication after EVAR;[7] however, only 22.8% of these patients received re-intervention. The second most common complication is type I endoleak, for which 65.8% of patients receive re-intervention. EVAR eligibility is based on instructions for use; small iliac vessel diameter (<7 mm) is often associated with Asian ethnicity or encountered in women.[8–10]

A new minimally invasive approach in the treatment of AAA, customised aortic repair (CAR), developed by TripleMed (Maastricht, The Netherlands) was recently introduced, as previously described by Bosman *et al.* and Doorschodt *et al.*[11–13] Two endovascular balloons are used to create flow lumens in the aneurysm sac. The aneurysm is then excluded from the blood flow by a complete seal with a non-contained, non-cross linked liquid polymer, with a curing time of about 5 min. After polymer curing, the balloons must be deflated and removed, leaving an aortic flow lumen in the polymer. There are similarities between CAR and the EndoVascular Aortic Sealing (EVAS), using the Nellix Endosystem (Endologix, Irvine, CA, USA); however, the absence of endobags and stent frames may simplify CAR.

The percutaneous CAR technique was tested by *in vivo* porcine experiments, by creating an aneurysm of a polyester tube graft, with promising results.[11] The low profile (6 Fr) endovascular balloons used for CAR may be a solution for patients with short necks, high angulation, and small iliac vessel diameters. The polymer mould may prevent type II endoleak.

However, the haemodynamically most favourable balloon configuration has not yet been established. As local haemodynamic factors are associated with clinical outcome,[14–17] velocity, vorticity, wall shear stress (WSS), and time averaged wall shear stress (TAWSS) were assessed using laser particle imaging velocimetry (PIV) for three different *in vitro* flow lumen configurations. Velocity was assessed because the fluid–solid interaction relates to displacement forces acting on the aortic wall or new lumen wall. Vorticity was assessed because alterations in local haemodynamics affect secondary flow patterns and WSS, which are associated with the origin of atherosclerosis and thrombosis. Low (time averaged) WSS is associated with the deposition of lipids, leading to the development of atherosclerotic lesions, while a high (time averaged) WSS is believed to be responsible for endothelial damage. Velocity and vorticity can be assessed *in vitro*, for comparison with clinical results. Owing to the fact that WSS is still a challenging parameter to obtain *in vivo* with current ultrasound, computed tomography, and magnetic resonance techniques it remains a non-clinical parameter for now.

METHODS

Flow models

Three custom made transparent polydimethylsiloxane (PDMS; Sylgard 184 [Dow Corning, Auburn, MI, USA]) flow models, based on the inverse negative mould of a three dimensional printed abdominal aortic aneurysm (AAA) model, previously described by Boersen *et al.*,[17] were used as *in vitro* models. The infrarenal neck diameter was 24 mm, infrarenal neck length 15 mm, and AAA diameter 55 mm.

Balloon designs

The first configuration, cross configuration (CC), is a combination of a full dog bone balloon (FDB; 200 × 10 mm) with a prefabricated thin skirt halfway and a half dog bone balloon (HDB; 120 × 10 mm [See Fig. 1A and 2A)]. The second configuration (PC1) consists of a FDB (200 × 10 mm) with a proximal skirt and a HDB (160 × 10 mm), as shown Fig. 1B. The third configuration (PC2) consists of a FDB (200 × 10 mm) with an elongated skirt and a HDB (160 × 10 mm; Fig. 1C).

Procedure

First, two guidewires (Terumo Europe, Leuven, Belgium) were placed in the suprarenal aortic lumen through both iliac arteries. The FDB was positioned in the aorta over the guidewire, at the origin of the lowest renal artery. The position was visually analysed, to prevent renal occlusion during filling of the aneurysm with polymer. For PC1 and PC2 the HDB was positioned directly below the bulb of the FDB. The distal part of the balloons ended in the common iliac artery. PDMS was chosen as a filling polymer as optical distortion had to be minimised for the laser PIV experiments. All balloons were pressurised up to one atmosphere while filling the aneurysm with PDMS. The models were placed in a depressurised oven for 12 h, at 60 °C to remove any remaining air bubbles and to cure the polymer.

After curing of the PDMS, the balloons were retracted from the newly created flow lumen. The models were installed in a flow set up, as previously described by Groot Jebbink,[18] consisting of a two element Windkessel set up with a pulsatile flow (60 beats/min, 90–120 mmHg, mean suprarenal inflow 1.6 L/min; range: 0.0–5.0 L/min). The four outflow vessels, two iliac and two renal arteries, all accounted for a quarter of the total outflow. The volumetric flow waveform was based on a study by Olufsen *et al.* and was also used for previous flow experiments.[17,19,20] Reproducibility of the measurements was analysed by comparison of the flow rate and flow velocity in the suprarenal aorta between models. The average and SD of WSS in the suprarenal region were assessed to obtain variability of the measurements.

A blood mimicking fluid (BMF) based on water, glycerol, and sodium iodide (47.4%, 36.9%, and 15.7%, respectively) with a dynamic viscosity of 4.3 mPas and a refractive index of 1.4, equal to PDMS, was used during flow experiments. Fluorescent particles (Rhodamine, size 1–20 μm, density 1190 kg/m^3 [Dantec Dynamics A/S, Skovlunde, Denmark]) were added to the BMF for the PIV measurements. A continuous wave laser (5 W DPSS laser, 532 nm [Cohlibri, Lightline, Germany]) was used to create a laser sheet that illuminated a narrow band of fluid. Perpendicular to the laser sheet, a high speed camera (FASTCAM SA-X2 [Photron, West Wycombe, UK]; 1000–3000 frames/s) captured the fluorescence signal emitted by the particles. An optical filter

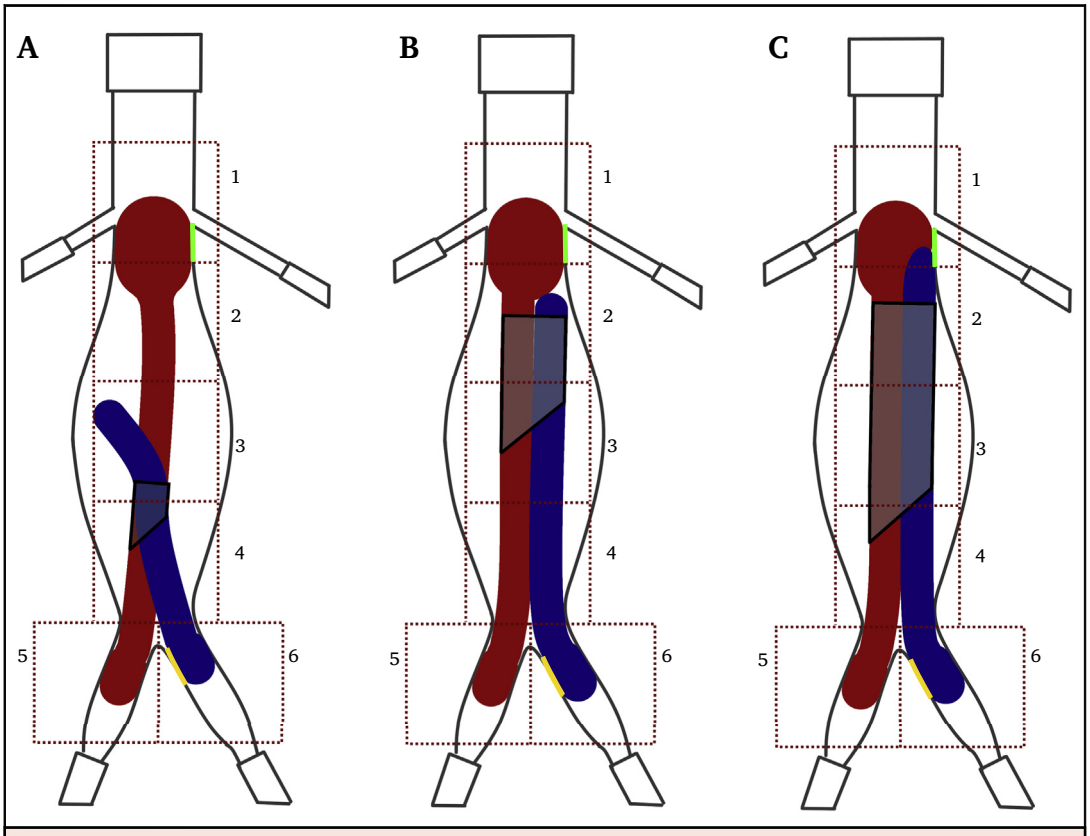

Figure 1. Schematic overview of the different balloon configurations to investigate haemodynamics in different lumen configurations. (A) Cross configuration (CC). The full dog bone (FDB) balloon (red) and half dog bone (HDB) balloon (blue) cross in the mid-segment of the aneurysm. A short skirt (black) holds the balloons together. (B) Parallel configuration 1 (PC1). The FDB (red) and HDB (blue) balloons are placed parallel to create a double 10 mm lumen. A short skirt directly below the bulb of the FDB (grey) is used to enable kissing balloons. (C) Parallel configuration 2 (PC2). The FDB (red) and HDB (blue) balloons are placed parallel to create a double 10 mm lumen. A longer skirt starting directly below the bulb of the FDB (black) to the mid lumen is used to enable kissing balloons over a long trajectory. The six regions of interest are numbered 1–6 and highlighted in red. Region 1 is the juxtarenal segment, region 2 the infrarenal segment, region 3 the cross section, region 4 the aortic bifurcation, and regions 5 and 6 are the left and right iliac segments, respectively. The segments used for wall shear stress and time averaged wall shear stress calculations are highlighted in the infrarenal neck (green) and medial wall of the left iliac (yellow).

was mounted to block reflections of the laser other than those of the particles. A window of approximately 30 × 30 mm was imaged onto the camera with a resolution of 1024 × 1024 pixels.

PIV analysis

The raw PIV data were first processed using background subtraction, adaptive thresholding, and masking to remove artifacts (Matlab 2016A; MathWorks, Natick, MA, USA). Edge detection was followed by fitting the contour of the lumen. Analysis was based on a cross correlation algorithm.[16,17]

The post-PIV data were averaged over 10 cardiac cycles to increase the signal to noise ratio and to calculate the average velocity vectors for a single cardiac cycle. The remaining end points, vorticity, WSS, and TAWSS were derived from the velocity data.

WSS was computed with an algorithm programmed in Matlab. The velocity magnitude at the wall was set at a no slip boundary condition, i.e. 0. Vorticity (ω) was defined as the curl of the flow velocity, u is the velocity vector ($\nabla \times u$). Normal values in the aortic arch and aneurysm sac range from −300/second up to 300/second during the cardiac cycle.[21–24]

The WSS (Pa) is expressed as the dynamic viscosity times the shear rate (s^{-1}), ($\tau_w = \mu \times \left(\frac{\partial u}{\partial y}\right)_{y=0}$) where μ is the dynamic viscosity, u the flow velocity parallel to the wall, and y the distance to the wall. After validation, flow and vorticity were displayed in Tecplot (Bellevue, WA, USA). The resulting cross sections were merged to create an overview of the flow in the whole configuration. The cross sections were not necessarily recorded at the same height, owing to the complex geometry of the configuration. The TAWSS was defined as the WSS averaged over one heart cycle, ($\frac{1}{T}\int_0^T |\tau_w| dt$) where T is the time in seconds and $\tau_w$the WSS. The segment directly below the left renal artery and the medial left iliac wall were used for the WSS and TAWSS calculations (Fig. 1). Minimum and maximum values of WSS and TAWSS were determined over the complete

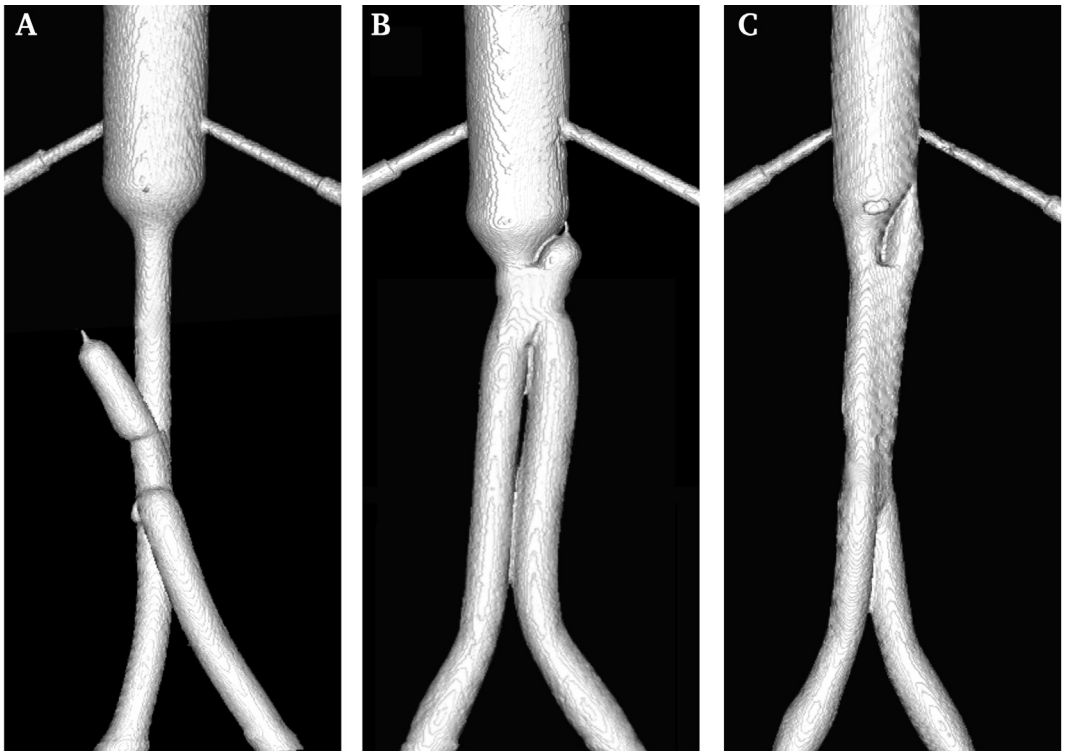

Figure 2. A reconstruction of the cone beam computed tomography data of the three configurations to investigate haemodynamics in different lumen configurations. (A) Cross configuration. (B) Parallel configuration 1. (C) Parallel configuration 2. The flow volume of the polymer mould, filled with air, clearly shows the differences in geometry between configurations.

segment and, again, not necessarily measured at the same location. Determination of WSS and TAWSS at the newly created polymer walls inside the flow lumen was not useful. Therefore, this study was mainly focused on flow velocities and vorticity for the regions within the new lumen.

RESULTS

Flow patterns

The velocity field maps are displayed per configuration in Figs 3 and 4. The vorticity fields are shown in Fig. 5, illustrating the complex flows in the infrarenal neck. Velocity, vorticity, WSS, and TAWSS per region per model are summarised in Fig. 6 (A — D). The velocity and vorticity fields of the three configurations over time are available in Video S1 (see Supplementary Material).

Supplementary videos related to this article can be found at doi:10.1016/j.ejvs.2018.11.012

The following is the supplementary data related to this article:Video 1Flow velocity during the cardiac cycle for the three configurations (CC, PC1, PC2).

Suprarenal flow was comparable for all models with an average flow rate of 1.62 ± 0.04 L/min (Fig. 3A). The mean ± SD of the flow velocities over 10 cardiac cycles in the lumen of the suprarenal aorta of the CC are displayed in Fig. 3B. The average and mean suprarenal WSS over 10 cardiac cycles was 0.043 Pa ± 0.0017 Pa, or 4.0% of the average WSS.

The diameters and surface of the suprarenal lumens were identical, 24.0 mm and 452.1 mm^2, respectively.

Assessment of the haemodynamics in the CC and PC1 models resulted in a new design of the balloon configurations, namely PC2. Although a decrease in vorticity in PC1 vs. the CC was observed, alterations to the skirt of the full dog bone balloon were thought to further improve the haemodynamics in the infrarenal neck. The new skirt was designed to assure that the HDB was positioned more proximally to increase the flow lumen surface and to create a smoother wall in the infrarenal neck compared with PC1 (Fig. 2B and C). In addition, the new skirt was designed to achieve a smoother transition from the two balloons in the infrarenal neck to the neo-bifurcation, and avoid a dead space between the balloons that remains after the curing of the polymer (Fig. 2B).

Cross configuration

The inflow trajectory of the CC (region of interest [ROI] 2), where the lumen narrows from 24 mm to 10.5 mm, showed high flow velocities both during peak and end systole (38 cm/s vs. −12 cm/s; see Fig. 6). Although the velocities were high, no vortices were observed. The two lumens of the balloons crossed in the aneurysmal sac (ROI 3), resulting in an increase of the mean surface from 91.2 mm^2 to 185.3 mm^2 (Fig. 4A). Flow velocities decreased to 23 cm/s in peak systole, leading to vortices and disturbed flow due to the sudden diameter increase. Vortices were directed into

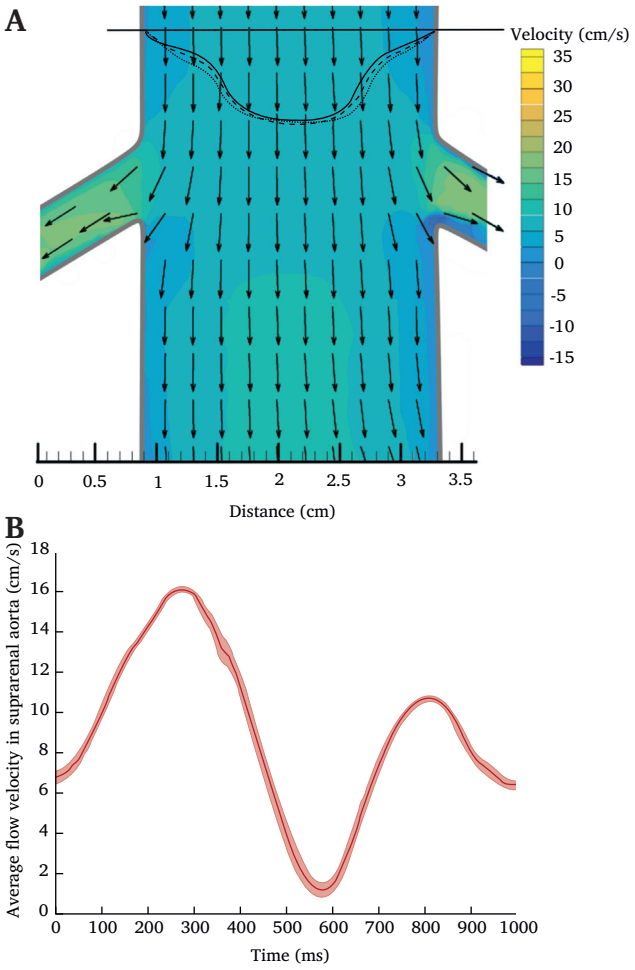

Figure 3. (A) Inflow profile of the cross configuration (line), parallel configuration 1 (dashed line) and parallel configuration 2 (dotted line) during peak systole. The flow profiles showed high similarities between the configurations. Profiles are obtained in region of interest 1, as depicted in Figure 1. (B) Flow velocity vs. time in the centre of the suprarenal aorta. The average velocity of 10 cardiac cycles is displayed, and measurement variability is plotted including 1 SD (shaded error).

the dead space, which protrudes from the HDB lumen (Fig. 5). Vorticity was high in the protruding lumen, ranging from −267/second to 337/second.

The WSS in the infrarenal neck was −0.29 Pa to 0.63 Pa, whereas TAWSS was almost zero (−0.05 Pa). The wall of the flow lumen was found to be somewhat irregular, owing to remnants of polymer between the balloons during curing. Distal to the crossing, high velocities were observed, up to 38 cm/s, whereas the contralateral lumen showed lower velocities, up to 18 cm/s during peak systole. However, the left and right outflows (ROI 5 and 6) showed only minor differences in flow velocities (peak systole: 12 cm/s; end systole: −4 cm/s) (see Video S1). WSS at the medial wall of the left iliac was −0.57 Pa to 0.82 Pa; the TAWSS was 0.31 Pa.

Supplementary Video 2 related to this article can be found at doi:10.1016/j.ejvs.2018.11.012.

The following is the supplementary data related to this article:Video 2Vorticity during the cardiac cycle for the three configurations (CC, PC1, PC2).

Parallel configurations: PC1

Flow velocities in the juxtarenal region (ROI 1) were 17 cm/s during peak systole and −5 cm/s during end systole (Fig. 4, Fig. S1 [see Supplementary Material]). Small vortices were only seen directly below the renal arteries. The infrarenal luminal surface narrowed from 453.0 mm^2 to 177.1 mm^2, and the velocities increased in both peak and end systole (23 cm/s vs. −10 cm/s; ROI 2), which is a decrease of 39.5% in peak velocity. Vortices were observed in the infrarenal neck (Fig. 5, Video S2). WSS in the infrarenal neck ranged from −0.86 Pa to 0.52 Pa; the TAWSS was 0.22 Pa. The zone of alignment of the two balloons, directly below the bulb of the FDB balloon, resulted in a narrowed lumen. Vorticity ranged from −194/s to 164/s, a difference of 6.5% and −18% vs. the CC. Continuing in the two separate lumens, flow patterns without vortices were seen during peak and end systole. Vorticity in this region (ROI 3) ranged from −112/s to 127/s, a decrease of 58.1% and 62.3% vs. the CC. During filling of the aneurysm with polymer, the two balloons "kissed" in the mid-segment of the aneurysm (ROI 3 and 4; Fig. 2). This resulted in a connection of 7−8 mm between the two flow lumens, as can be seen in Fig. 2B. During end systole, BMF flowed backwards from the left lumen to the right lumen, the other way around during peak systole (see Video S1).

The flow in the left iliac was up to 16 cm/s during peak systole and −12 cm/s during end systole, 25% and 50%, respectively, higher than for the other two configurations (Fig. S1).

WSS ranged from −1.23 Pa to 1.06 Pa for the medial iliac segment, an increase of 115.8% and 29.3%, respectively. TAWSS was 0.48 Pa (Fig. 6D), an increase of 54.8%. The flow was directed to the inner wall, owing to the bending of the iliac wall during the peak systole. During end systole, the highest flow was seen at the outer wall.

Parallel configurations: PC2

Maximum observed velocity in the infrarenal neck was 23 cm/s in peak systole, whereas it was −9 cm/s during end systole, comparable to PC1 (Fig. 4C). Vorticity ranged from −109/s to 98/s, a decrease of 43.8% and 40.2%, respectively, compared with PC1. The luminal surface narrowed in the infrarenal region from 451.5 mm^2 to 214.2 mm^2, an increase of 20.9% compared with PC1. During the procedure, the balloons tilted slightly, resulting in the lumens not being parallel in a sagittal view of the model. In the mid-segment of the aneurysm (ROI 2), were the lumen narrowed slightly, the velocities were higher, 24 cm/s and −4 cm/s, respectively (Fig. 6A). The vorticity for this segment (−118/s to 112/s) differed +5.4% and −11.8%, respectively, compared with the PC1 configuration. No vortices were observed during the complete cardiac cycle, whereas they were clearly present in the PC1 configuration. The neo-bifurcation (ROI 4), where the lumen splits into the left and right iliac artery, was more tapered than PC1.

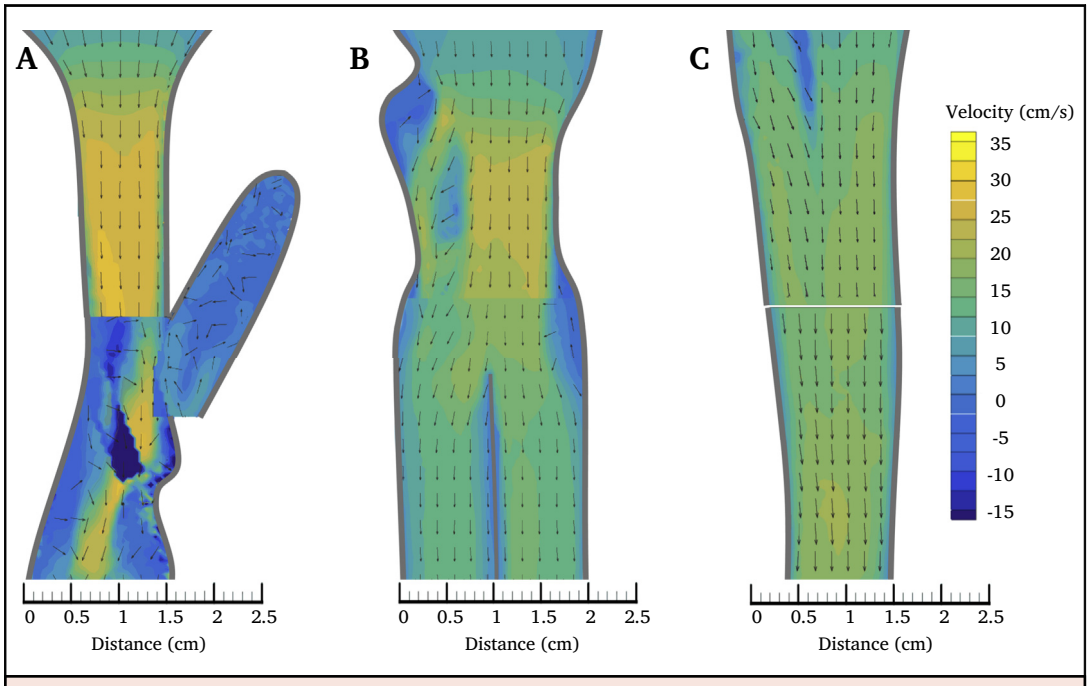

Figure 4. Flow velocity in the region where the balloons are positioned together in the skirt for the (A) cross configuration, (B) parallel configuration 1, and (C) parallel configuration 2 during peak systole. Large differences in infrarenal flow velocities are observed between the configurations.

WSS ranged from −0.88 Pa to 0.91 Pa, a decrease of 28.5% and 14.2%, respectively, compared with PC1.

The TAWSS at the inner wall of the left iliac artery was 0.38 Pa, a decrease of 20.8% compared with PC1 (Fig. 6D). Outflow velocity was 12 cm/s during peak systole and −6 cm/s during end systole, comparable with the CC (Fig. S1).

DISCUSSION

This study investigated the haemodynamics in CAR, a novel concept for treating AAA. Haemodynamics, in particular vorticity, seemed to be more favourable in the PC2 configuration. Comparing the configurations showed that the CC developed most vortices, mainly in the infrarenal (ROI 2) and mid-aneurysm (ROI 3) segment, followed by PC1.

Balloon concepts

This study investigated the haemodynamics of three configurations, CC, PC1, and PC2. The advantage of the CC is the "one size fits all" solution. Only the FDB has to be sized based on the patient's anatomy (length and diameter), the protruding part of the HDB can vary in length. To avoid the narrowing in the infrarenal neck (ROI 2) and the protruding "dead space", the concept of two parallel balloons aligned in the

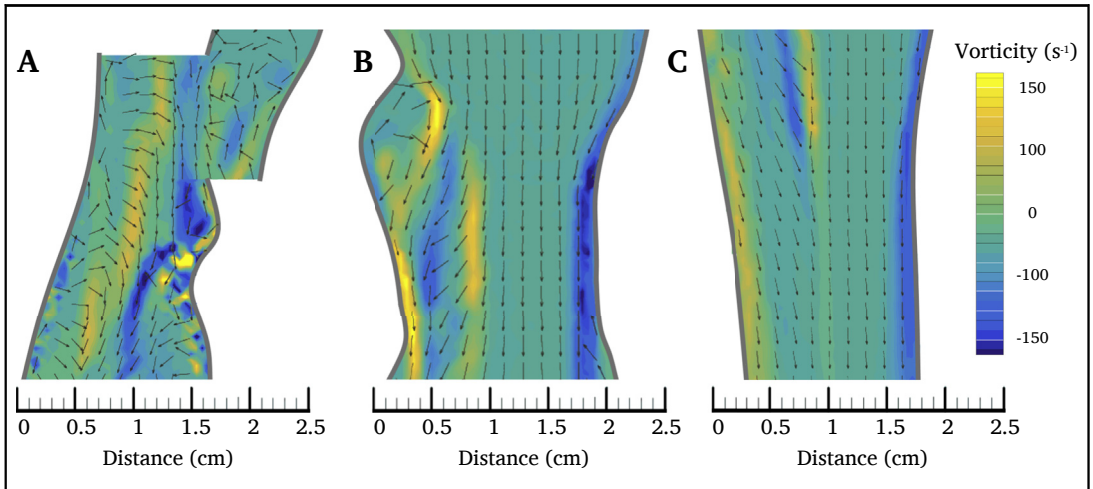

Figure 5. Vorticity in the region were the balloons crossed for (A) cross configuration (CC), (B) parallel configuration (PC) 1; and (C) PC2 during peak systole. Vortices are observed in this region, especially in the CC and PC, and visualised in Video S2.

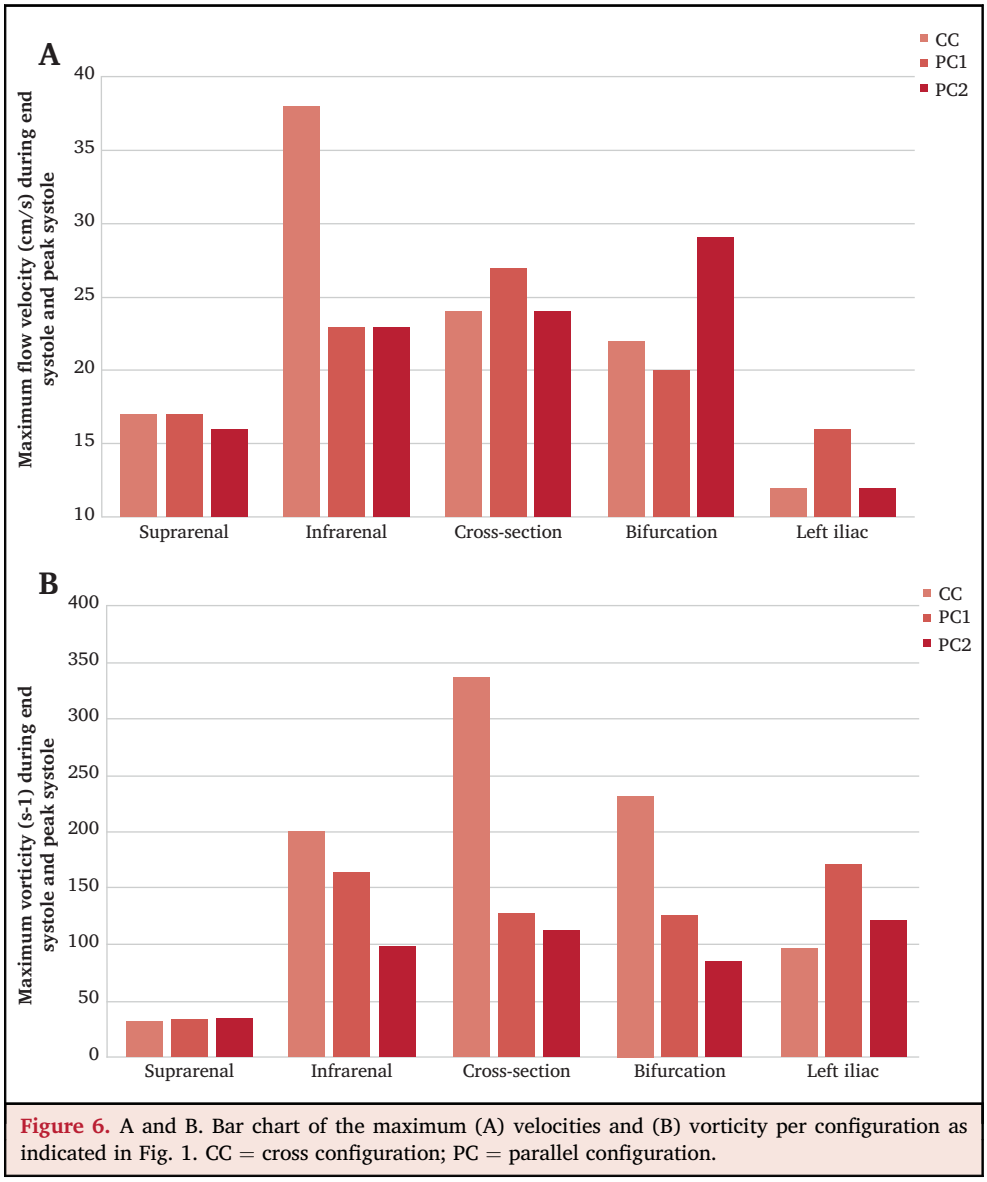

Figure 6. A and B. Bar chart of the maximum (A) velocities and (B) vorticity per configuration as indicated in Fig. 1. CC = cross configuration; PC = parallel configuration.

infrarenal neck was developed. Depending on the patients' anatomy, various balloon lengths have to be on the shelf while planning the procedure. By improving the conformation of the balloons in the infrarenal neck in PC2, the minimum surface area of the lumen increased from 89.3 mm^2 (CC) to 177.1 mm^2 (PC1) to 214.2 mm^2 (PC2), thereby decreasing the corresponding flow velocities and shear stresses. The HDB is placed caudal to the FDB bulb, not parallel like chimney EVAR, to assure perfect sealing in the aortic neck and prevent leakage of polymer into the flow lumen.

The design of the skirt of the FDB in PC2, based on the outcomes of PC1, resulted in a predictable figure of eight shape of the two "kissing" lumens. As the balloons are inflated to one atmosphere of pressure, the two balloons become non-deformable, resulting in a predictable geometry of the lumens. The HDB is slightly oversized compared with the FDB skirt, assuring a fixed position of the balloons when inflated. Full deployment of the balloons during the procedure should be examined under fluoroscopy by using a contrast saline solution for inflation.

Haemodynamics

The early stages of atherosclerosis and plaque formation are thought to be associated with regions of low WSS (10^{-2} Pa), as a result of alternated flow patterns.[21,25,26] In the present study all measured parameters were above this threshold value. However, the interpretation of the used metrics, such as WSS and TAWSS, is often inconclusive and less robust than commonly assumed.[15] Therefore, the four end points were mainly used for a direct comparison between the different configurations.

Earlier studies pointed out that flow in the abdominal aorta is non-laminar, and include vortices and recirculation zones, especially in AAA.[21,24,27] Disturbed flow can result in increasing stresses acting on the aneurysm wall and may be

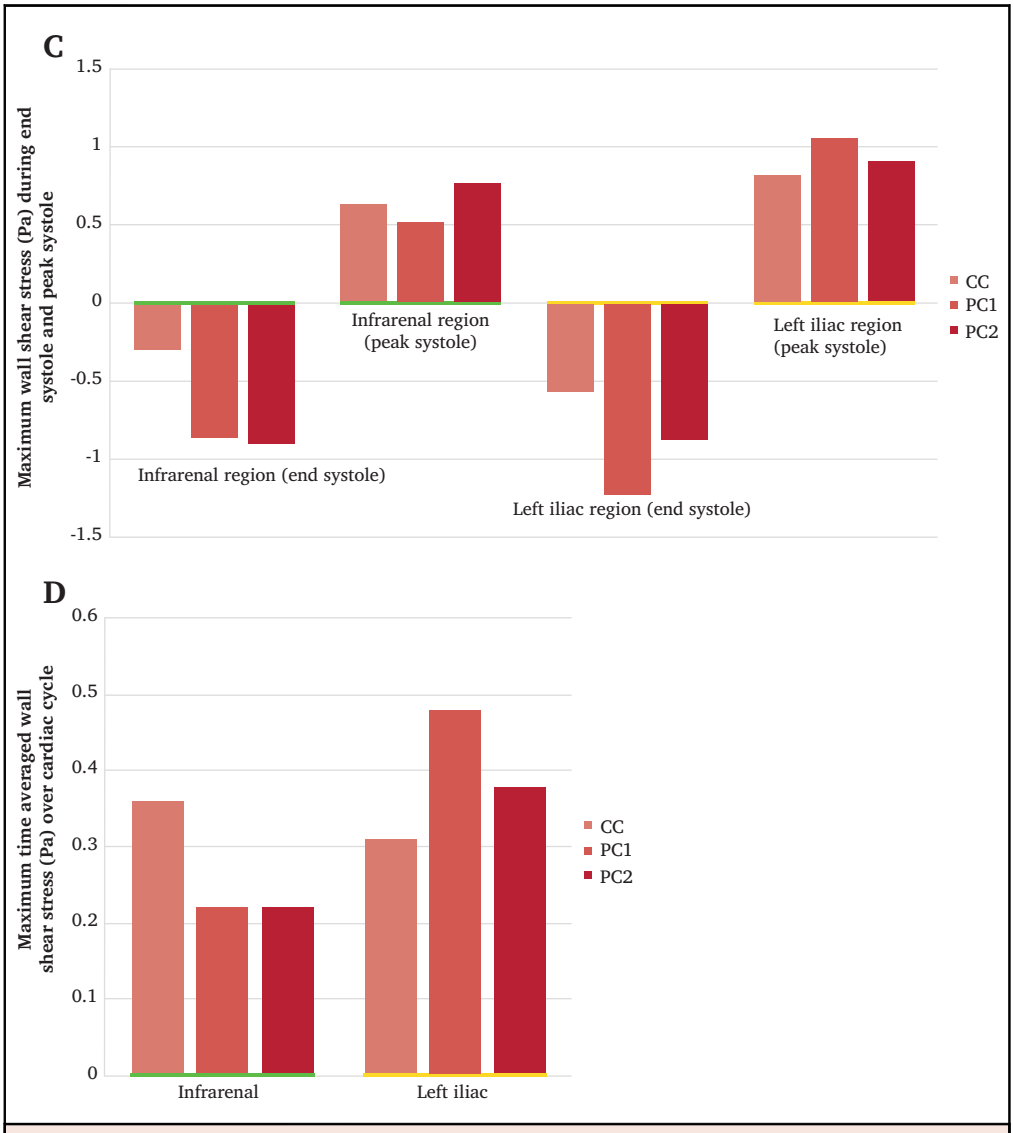

Figure 6. (*continued*). C and D. Bar chart of the maximum (C) wall shear stress during end systole and peak systole, and (D) time averaged wall shear stress over the cardiac cycle, per region (green and yellow, as indicated in Fig. 1), per configuration. CC = cross configuration; PC = parallel configuration.

responsible for further aortic dilatation.[28] Therefore, excluding the aneurysm sac from the arterial circulation, for example during EVAR, should minimise complex flows at the inflow and outflow segments of the stent at healthy aortic wall.

Vorticity was used as a quantity to assess haemodynamic differences between configurations. Several authors have studied haemodynamics focusing on vorticity in the aortic arch or in the aneurysm sac and found values ranging from −300/s to 300/s during the cardiac cycle to be typical.[21–24] In particular, regions with irregular walls, such as the crossing section and the "dead" space, are prone to develop regions of both high and low shear stress and vortices. Interestingly, vortices developed in the crossing area of PC1, repeated caudally and dissipated mid lumen (ROI 3; Video S1). Combination of high shear rates (>5000/s) and vortices activates platelets and may result in thrombogenic and inflammatory responses in regions with a high residence time. Although shear rates above the pathological threshold of >5000/s were not measured in this study, vorticities close to or above threshold (−300/s to 300/s) were observed in the CC. These observations highlighted the importance of designing smooth proximal neck geometry in CAR.

The lumen of the CC narrowed from 24 mm to 10 mm in diameter, resulting in flow velocities up to 38 cm/s. At the crossing section of the two lumens, a sudden expansion of the flow lumen (2 × 10 mm) resulted in the generation of vortices. These currents were directed into the protruding part of the lumen, a blind cavity. The BMF used in this study has no thrombotic characteristics; therefore, the flow remained in this cavity. Based on the observed low flow velocities, blood clots may form in an *in vivo* situation, thereby filling the cavity, and from which (micro) thrombi may enter the bloodstream and cause a peripheral thromboembolism.[29,30]

A direct comparison of the outflow through the left common iliac artery (ROI 6) lumen was also of interest, as altered flow patterns may result in changed WSS of the healthy peripheral vessel wall. The velocity and vorticity, and resulting WSS and TAWSS, were higher in PC1. The flow was predominantly directed towards the left iliac artery as a result of the geometry of the lumens in the infrarenal neck.

Limitations

PDMS was used for the experiments instead of the CAR manufacturer's polymer as optical access was needed for the laser PIV measurements. However, the differences in the mechanical properties between the two polymers are small and not expected to change the observed flow profiles.[11,31] The PDMS walls of the models were considered to be rigid. Although this affects the results in the regions without polymer, it was assumed that the influence on flow characteristics was limited as the vasculature of this patient population is stiffened by atherosclerotic disease.[32,33]

Interpretation of the observed flow patterns, especially cross sections displaying vortices, is challenging. A direct comparison was sometimes difficult, as each geometry of the models is unique. In addition, complex three dimensional haemodynamic flows are assessed in a two dimensional configuration, with in and out of plane motion, and which complicated analysis of the flow patterns.

The tortuous geometry made wall detection challenging, which may have affected the accuracy of WSS calculations. A total flow rate of 1.6 L/min was used in all models, although being physiological, this was at the lower boundary of what is seen in patients.

There are similarities between CAR and the Nellix endosystem, especially the complete filling of the aneurysm sac using a polymer, creating an increased mass of the system compared with EVAR. Owing to the increased mass the resonance frequency of system is lowered to within the frequency range of vibrations induced during daily activities.[34] For the Nellix endosystem this mechanism may promote lateral displacement or bending of the stents if insufficient polymer surrounds them, potentially resulting in caudal migration of the endosystem.[35] Although the described failure mechanism may be applicable to CAR, important distinctions have to be made. First, CAR does not incorporate stent frames and endobags, as with the Nellix endosystem; it is a one piece polymer only solution. Second, CAR fixation differs from that of the Nellix endosystem. The low viscosity polymer moulds to the morphology of the aneurysm sac instead of using pressurised smooth endobags, which are mainly fixed on the aortic bifurcation.

Flow recirculation in the Nellix endosystem has been suggested as a potential risk of distal embolisation by Boersen *et al.*,[36] due to the "drooling shoulders" of the endobags. The tapered design of the FDB in CAR enhances a smooth inflow of blood into the newly created lumen, preventing recirculation zones. However, loss of proximal and distal seal between polymer and aortic wall, because of the thinning layer of polymer towards the edges, remains a potential risk and may cause type Ia/b endoleak. This may be a result of caudal migration of the polymer and/or dilation of the aortic neck as a result of disease progression. Deployment of a self expanding stent covering the tapered edges of the cast, as described by Doorschodt *et al.*,[13] may prevent non-apposition between polymer and aortic wall.

Future research will be focused on the identification of the instructions for use and the clinical introduction of CAR, focused on two indications: first, the standalone (percutaneous) use of CAR in the treatment of AAA; and, second, the use of CAR in the treatment of persistent type II endoleak, by filling the aneurysm sac surrounding the primary endograft. The potential failure mechanisms, highlighted by Argani *et al.*,[34] will be incorporated in this research plan.

CONCLUSIONS

The flow lumens created by three balloon configurations used in an *in vitro* model of CAR have been studied, and resulted in different haemodynamics. The differences in velocities and lower vorticity, especially at the crossing section of the two balloons, showed that PC2 has favourable haemodynamics compared with the CC and PC1. Future research will be focused on the clinical applicability of CAR based on the design of PC2.

CONFLICT OF INTEREST

None.

FUNDING

Non-restricted grant by TripleMed B.V. Maastricht, Netherlands.

APPENDIX A. SUPPLEMENTARY DATA

Supplementary data to this article can be found online at https://doi.org/10.1016/j.ejvs.2018.11.012.

REFERENCES

1 Parodi JC, Palmaz JC, Barone HD. Transfemoral intraluminal graft implantation for abdominal aortic aneurysms. *Ann Vasc Surg* 1991;**5**:491–9.
2 Cieri E, De Rango P, Cao P. Effect of stentgraft model on aneurysm shrinkage in 1,450 endovascular aortic repairs. *Eur J Vasc Endovasc Surg* 2013;**46**:192–200.
3 Pintoux D, Chaillou P, Gouëffic Y. Long-term influence of suprarenal or infrarenal fixation on proximal neck dilatation and stentgraft migration after EVAR. *Ann Vasc Surg* 2011;**25**:1012–9.
4 Vandy F, Upchurch GR. Endovascular aneurysm repair: current status. *Circ Cardiovasc Interv* 2012;**5**:871–82.
5 Tadros RO, Faries PL, Ellozy SH, Lookstein RA, Vouyouka AG, Schrier R, et al. The impact of stent graft evolution on the results of endovascular abdominal aortic aneurysm repair. *J Vasc Surg* 2014;**59**:1518–27.
6 Patel R, Sweeting MJ, Powell JT, Greenhalgh RM. Endovascular versus open repair of abdominal aortic aneurysm in 15-years' follow-up of the UK endovascular aneurysm repair trial 1 (EVAR trial 1): a randomised controlled trial. *Lancet* 2016;**388**:2366–74.
7 Powell JT, Sweeting MJ, Ulug P, Blankensteijn JD, Lederle FA, Becquemin JP, et al. Meta-analysis of individual-patient data from EVAR-1, DREAM, OVER and ACE trials comparing outcomes of

endovascular or open repair for abdominal aortic aneurysm over 5 years. *Br J Surg* 2017;**104**:166–78.
8 Sweet MP, Fillinger MF, Morrison TM, Abel D. The influence of gender and aortic aneurysm size on eligibility for endovascular abdominal aortic aneurysm repair. *J Vasc Surg* 2011;**54**:931–7.
9 Masuda EM, Caps MT, Singh N, Yorita K, Schneider PA, Sato DT, et al. Effect of ethnicity on access and device complications during endovascular aneurysm repair. *J Vasc Surg* 2004;**40**:24–9.
10 Park KH, Lim C, Lee JH, Yoo JS. Suitability of endovascular repair with current stent grafts for abdominal aortic aneurysm in Korean patients. *J Korean Med Sci* 2011;**26**:1047–51.
11 Bosman WMPF, Vlot J, Van Der Steenhoven TJ, Van Den Berg O, Hamming JF, De Vries AC, et al. Aortic customize: an in vivo feasibility study of a percutaneous technique for the repair of aortic aneurysms using injectable elastomer. *Eur J Vasc Endovasc Surg* 2010;**40**:65–70.
12 Bosman W-MPF, Hinnen J-W, van der Steenhoven TJ, de Vries AC, Brom HLF, Jacobs MJ, et al. Treatment of types II–IV endoleaks by injecting biocompatible elastomer (PDMS) in the aneurysm sac: an in vitro study. *J Endovasc Ther* 2011;**18**:205–13.
13 Doorschodt BM, Brom HL, de Vries AC, Meers C, Jacobs MJ. In vivo evaluation of customized aortic repair using a novel survival model. *Eur J Vasc Endovasc Surg* 2016;**52**:166–72.
14 Koskinas KC, Chatzizisis YS, Antoniadis AP, Giannoglou GD. Role of endothelial shear stress in stent restenosis and thrombosis: pathophysiologic mechanisms and implications for clinical translation. *J Am Coll Cardiol* 2012;**59**:1337–49.
15 Peiffer V, Sherwin SJ, Weinberg PD. Does low and oscillatory wall shear stress correlate spatially with early atherosclerosis? A systematic review. *Cardiovasc Res* 2013;**99**:242–50.
16 van de Velde L, Donselaar EJ, Groot Jebbink E, Boersen JT, Lajoinie GPR, de Vries JPPM, et al. Partial renal coverage in endovascular aneurysm repair causes unfavorable renal flow patterns in an infrarenal aneurysm model. *J Vasc Surg* 2018;**67**:1585–94.
17 Boersen JT, Groot Jebbink E, Versluis M, Slump CH, Ku DN, de Vries JPPM, et al. Flow and wall shear stress characterization after endovascular aneurysm repair and endovascular aneurysm sealing in an infrarenal aneurysm model. *J Vasc Surg* 2017;**66**:1844–53.
18 Groot Jebbink E. *Innovation in Aortoiliac Stenting: an in Vitro Comparison*. MSc Thesis. University of Twente; 2014.
19 Olufsen MS, Peskin CS, Kim WY, Pedersen EM, Nadim A, Larsen J. Numerical simulation and experimental validation of blood flow in arteries with structured-tree outflow conditions. *Ann Biomed Eng* 2000;**28**:1281–99.
20 Groot Jebbink E, Grimme F a B, Goverde PCJM, van Oostayen JA, Slump CH, Reijnen MMPJ. Geometrical consequences of kissing stents and the covered endovascular reconstruction of the aortic bifurcation configuration in an in vitro model for endovascular reconstruction of aortic bifurcation. *J Vasc Surg* 2015;**61**:1306–11.
21 Von Spiczak J, Crelier G, Giese D, Kozerke S, Maintz D, Bunck AC. Quantitative analysis of vortical blood flow in the thoracic aorta using 4D phase contrast MRI. *PLoS One* 2015;**10**:1–19.
22 Gur H Ben, Brand M, Kósa G, Brand M, Kósa G. *Computational fluid dynamics of blood flow in the the abdominal fluid aorta post " chimney " endovascular aneursm repair (ChEVAR)*. February 22 2017. Available at: https://www.intechopen.com/books/aortic-aneurysm/computational-fluid-dynamics-of-blood-flow-in-the-abdominal-aorta-post-chimney-endovascular-aneurysm.
23 Büsen M, Kaufmann TAS, Neidlin M, Steinseifer U, Sonntag SJ. In vitro flow investigations in the aortic arch during cardiopulmonary bypass with stereo-PIV. *J Biomech* 2015;**48**:2005–11.
24 Biasetti J, Hussain F, Gasser TC. Blood flow and coherent vortices in the normal and aneurysmatic aortas: a fluid dynamical approach to intra-luminal thrombus formation. *J R Soc Interf* 2011;**8**:1449–61.
25 Zarins CK, Giddens DP, Bharadvaj BK, Sottiurai VS, Mabon RF, Gladov S, et al. Carotid bifurcation atherosclerosis: quantitative correlation of plaque localization with flow velocity profiles and wall shear stress. *Circ Res* 1983;**53**:502–14.
26 Ku DN, Giddens DP, Zarins CK, Glagov S. Pulsatile flow and atherosclerosis in the human carotid bifurcation positive correlation between plaque location and low and oscillating shear stress. *Arterioscler Thromb Vasc Biol* 1985;**5**:293–302.
27 Bernad SI, Bernad E., Barbat T, Brisan C, Albulescu V. An analysis of blood flow dynamics in AAA. Available at: https://www.intechopen.com/books/etiology-pathogenesis-and-pathophysiology-of-aortic-aneurysms-and-aneurysm-rupture/an-analysis-of-blood-flow-dynamics-in-aaa.
28 Khanafer KM, Bull JL, Upchurch GR, Berguer R. Turbulence significantly increases pressure and fluid shear stress in an aortic aneurysm model under resting and exercise flow conditions. *Ann Vasc Surg* 2007;**21**:67–74.
29 Menichini C, Xu XY. Mathematical modeling of thrombus formation in idealized models of aortic dissection: initial findings and potential applications. *J Math Biol* 2016;**73**:1205–26.
30 Rayz VL, Boussel L, Ge L, Leach JR, Martin AJ, Lawton MT, et al. Flow residence time and regions of intraluminal thrombus deposition in intracranial aneurysms. *Ann Biomed Eng* 2010;**38**:3058–69.
31 Dow Corning Corp. Product information – 184 silicone elastomer. Available from: https://consumer.dow.com/en-us/document-viewer.html?ramdomVar=7626443017551882 47&docPath=/content/dam/dcc/documents/en-us/productdatasheet/11/11-31/11-3184-sylgard-184-elastomer.pdf.
32 Perktold K, Rappitsch G. Computer-simulation of local blood-flow and vessel mechanics in a compliant carotid-artery bifurcation model. *J Biomech* 1995;**28**:845–56.
33 Kabinejadian F, Cui F, Leo HL. Effects of a carotid covered stent with a novel membrane design on the blood flow regime and hemodynamic parameters distribution at the carotid artery bifurcation. *Med Biol Eng Comput* 2014;**53**:165–77.
34 Argani LP, Torella F, Fisher RK, McWilliams RG, Wall ML, Movchan AB. Abdominal aortic aneurysms and endovascular sealing: deformation and dynamic response. *Sci Rep* 2017;**7**:1–17.
35 Carpenter JP, Lane JS, Trani J, Hussain S, Healey C, Buckley CJ, et al. Refinement of anatomic indications for the Nellix System for endovascular aneurysm sealing based on 2-year outcomes from the EVAS FORWARD IDE trial. *J Vasc Surg* 2018;**68**:720–730.e1.
36 Boersen JT, Groot Jebbink E, Van de Velde L, Versluis M, Lajoinie G, Slump CH, et al. The influence of positioning of the Nellix endovascular aneurysm sealing system on suprarenal and renal flow: an in vitro study. *JEVT* 2017;**24**:677–87.